Ellipsometric Measurements of the Thermal Stability of Alternative Fuels

Leigh Nash
Center for Advanced Turbomachinery and Energy Research (CATER),
Mechanical and Aerospace Engineering,
University of Central Florida,
Orlando, FL 32816

Jennifer Klettlinger
NASA Glenn Research Center,
Cleveland, OH 44135

Subith Vasu
Center for Advanced Turbomachinery and Energy Research (CATER),
Mechanical and Aerospace Engineering,
University of Central Florida,
Orlando, FL 32816

Thermal stability is an important characteristic of alternative fuels that must be evaluated before they can be used in aviation engines. Thermal stability refers to the degree to which a fuel breaks down when it is heated prior to combustion. This characteristic is of great importance to the effectiveness of the fuel as a coolant and to the engine's combustion performance. The thermal stability of Sasol iso-paraffinic kerosene (IPK), a synthetic alternative to Jet-A, with varying levels of naphthalene has been studied on aluminum and stainless steel substrates at 300–400 °C. This was conducted using a spectroscopic ellipsometer to measure the thickness of deposits left on the heated substrates. Ellipsometry is an optical technique that measures the changes in a light beam's polarization and intensity after it reflects from a thin film to determine the film's physical and optical properties. It was observed that, as would be expected, increasing the temperature minimally increased the deposit thickness for a constant concentration of naphthalene on both substrates. The repeatability of these measurements was verified using multiple trials at identical test conditions. Finally, the effect of increasing the naphthalene concentration at a constant temperature was found to also minimally increase the deposit thickness.
[DOI: 10.1115/1.4036961]

Introduction

Alternative jet fuels are of interest to the aviation community because of rising oil costs, the need to secure a consistent oil supply, and the desire for cleaner burning engines [1–5]. Alternative fuels are an important part of the plan to achieve these desires [6,7]. However, before an alternative fuel can be used, it must be comprehensively tested for its compatibility with existing infrastructure, engine architecture, combustion, and emission [8–11], and the infrastructure for its implementation must be built [12]. An important fuel property that must be characterized is the thermal stability [13], which is a measure of the degree to which a fuel breaks down when it is heated. As a weight and space saving measure, the fuel in an aircraft is used as engine coolant in addition to being the propellant. Preheating the fuel can cause it to break down inside the engine pluming, fouling the lines and leading to a loss of fuel flow. Knowledge of the way a fuel thermally decomposes and the amount of deposit that is formed is essential for anticipating maintenance schedules and possible fuel flow issues. A basic level of thermal stability is also required of all alternative fuels for adoption as acceptable jet fuels.

In the past, the ASTM Standard Test Method for Thermal Oxidation Stability of Aviation Turbine Fuels (D3241), also known as the Jet Fuel Thermal Oxidation Test (JFTOT), relied solely on a comparison between a color standard and the deposits left on a heated tube after the fuel was flowed over it to determine thermal stability. A fuel was defined as thermally stable at a particular temperature if the deposit rated a 3 or less on the color scale [14] shown in Fig. 1. The tubes were placed into a lighted box called the visual tube rater, and an operator would compare the color of the deposit on the tube to the color standard to determine the most appropriate rating. These comparisons were deemed to be subjective and nonrepeatable [15], which lead to the implementation of ellipsometry to measure film deposit thicknesses [16].

Ellipsometry allows objective measurements of the film thickness to be made, yielding quantitative data that can be statistically analyzed, which is not true of the color standard. In addition, the color standard is only applicable to conventional fuels on aluminum substrates. Ellipsometry is more versatile in that it can be used to analyze the sample regardless of the composition of the film or the substrate. Significant details about the film are lost when the tube is assigned a color rating. Small changes to the film that do not manifest themselves as a color change are lost in this way, but are detectable by ellipsometry. The ellipsometric thermal stability criteria requires the thickest part of the deposit be less than 85 nm in thickness, and this technique is sensitive to minute changes in the deposit thickness, making it extremely precise.

Sasol iso-paraffinic kerosene (IPK) is a Fisher–Tropsch synthetic jet fuel. This alternative fuel is composed of greater than 90% C_{10} and C_{12} iso-paraffins [17], and it contains far fewer components than traditional fuels which can have hundreds of components. A typical IPK fuel produced by Sasol contains 2.6% cycloparaffins, and 97.4% n- and iso-paraffins [18]. The additive tested in this work is naphthalene, a two-ringed aromatic structure with the formula $C_{10}H_8$. Naphthalene is added to improve a fuel's

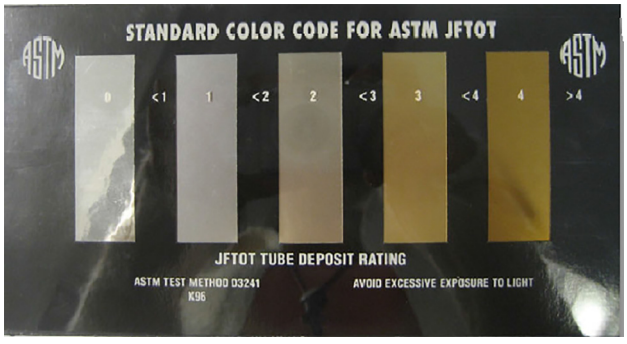

Fig. 1 JFTOT color standard adapted from Ref. [16]. There are ten designations including 0, <1, 1, <2, 2, <3, 3, <4, 4, and >4. The 0 rating corresponds to a clean tube, and the deposit gets darker as the rating number increases.

Contributed by the Advanced Energy Systems Division of ASME for publication in the Journal of Energy Resources Technology. Manuscript received April 14, 2017; final manuscript received April 18, 2017; published online July 17, 2017. Editor: Hameed Metghalchi.

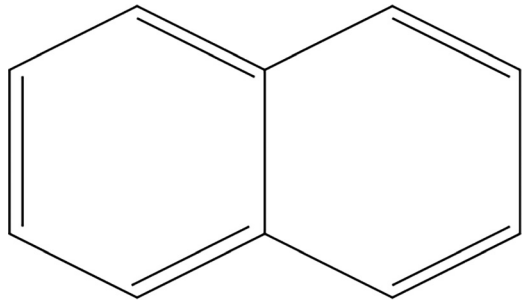

Fig. 2 Naphthalene structure. Naphthalene is a two-ringed aromatic compound with the formula $C_{10}H_8$.

auto-ignition resistance for safety reasons and its structure can be seen in Fig. 2.

Sasol IPK is produced using the Fischer–Tropsch process from gasified coal [19]. Other aspects of such gas to liquid fuels including laminar burning speeds and ignition delay times have been studied previously [20]. The first step in the Fischer–Tropsch process is to gasify the coal to produce syn-gas. The syn-gas is then converted into crude oil and then separated into usable fuels. Paraffin wax, an olefin light oil, and water are produced through the following reaction steps [21]:

$$2H_2 + CO \rightarrow CH_2 + H_2O \quad (1)$$

$$(2n+1)H_2 + nCO \rightarrow C_nH_{2n+2} + nH_2O \quad (2)$$

$$2nH_2 + nCO \rightarrow C_nH_{2n} + nH_2O \quad (3)$$

$$CO + H_2O \leftrightarrow CO_2 + H_2 \quad (4)$$

Equation (1) is the global Fischer–Tropsch reaction, Eq. (2) is the paraffin producing reaction, Eq. (3) produces the olefins, and Eq. (4) is the water gas shift reaction.

Experimental Method

Using the color standard to define the thermal stability of a fuel yields only a rating of the color of the deposit. Although the darker colors loosely correlate with thicker deposits, this rating has been demonstrated to be subjective, and it is difficult to perform meaningful analysis on a qualitative rating. In addition, the color categories are broad, and nuanced details about the deposit are lost when the color rating is applied. Samples that receive the same color rating may have important differences between them. Ellipsometric analysis, on the other hand, produces numerical values for the deposit's thickness profile. This is an objective test that yields numerical data which is precise, so that differences between samples that would have received the same color rating can be analyzed. Ellipsometry can also be used to study the roughness of a surface, the composition of the sample, and the optical constants of the material in addition to the thickness. In this study, the thickness is reported because it is the parameter chosen to represent the thermal stability in the ASTM standard. Thermal stability is inherently challenging to measure, because it must be measured indirectly, either by the color or by thickness of a deposit.

The samples were prepared using an Alcor hot liquid process simulator (HLPS) model HLPS-400, following the JFTOT procedure given in ASTM D3241. A schematic of the HLPS can be seen in Fig. 3. The tube is placed into the HLPS and resistively heated to the test temperature. The standard requires that an acceptable fuel be stable at least at 260 °C, so testing begins at this point. In this particular study, the test temperature started at 300 °C because the alternative fuels do not begin to break down below this point. The fuel is flowed through a cylindrical annulus surrounding the test tube at a rate of 3 cm^3/min for 150 mins. Then the tube is removed from the HLPS and allowed to cool. Any deposit on the tube is compared to the color standard and the tube is given a numerical rating from 0 to 4. If the tube receives a passing rating ($\leq$3), the test temperature is increased by 5 °C and the test is run again, starting with a new clean tube. Once the tube fails, the highest passing temperature is defined as the thermal breakpoint of the fuel. This completes the traditional JFTOT procedure. The ellipsometric measurements are made after the conclusion of the traditional JFTOT.

A Horiba Scientific spectroscopic ellipsometer (Auto SE) was used to make the ellipsometric measurements presented in this study. The Auto SE has a spectral range of 400–1100 nm and 70 deg angle of incidence. The sample viewer is a CCD camera with a field of view of 1.33 by 1 mm and a resolution of 10 μm. A small spot size was used in order to minimize the effect of the tubes' curved surfaces. In the most basic sense, an ellipsometer is made up of a light source, polarizer, detector, and analyzer. After leaving the source, the light is given a linear polarization. The light then encounters the sample. After reflection from the film, it is elliptically polarized, and it enters the detector (illustrated in Fig. 4). The polarization can be explained if the light is imagined as a series of rays oscillating up and down, with the amplitude of the rays changing to follow the path of the wave. If these rays are viewed normal to the direction in which they are moving, they trace out the shape of an ellipse when the light is elliptically polarized. The shape of this ellipse indicates the amplitude and the phase of the components of the light traveling parallel and perpendicular to the plane of incidence, which are the parameters

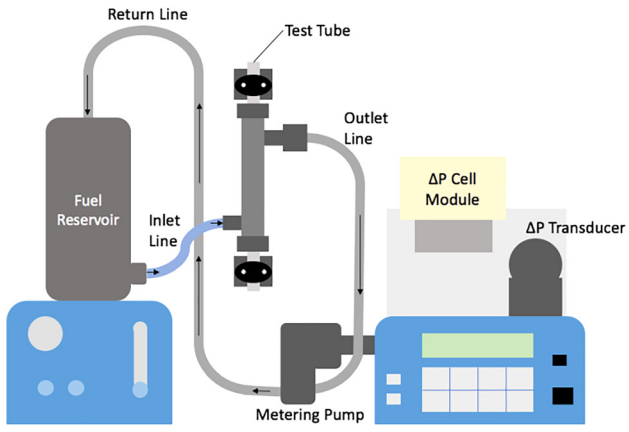

Fig. 3 Hot liquid process simulator schematic. Fuel is pumped out of the reservoir, over the test tube, and then back into the reservoir at a rate controlled by the metering pump.

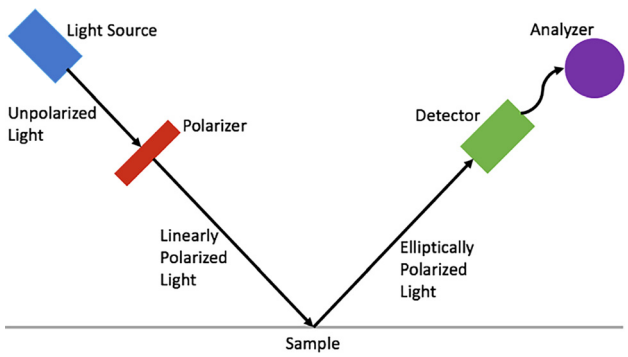

Fig. 4 Primary components of the ellipsometer. Unpolarized light is generated by the light source and then linearly polarized. After the light reflects off of the sample, it is elliptically polarized and is collected by the detector. Finally, the signal from the detector is analyzed to determine the amplitude and phase of the light's components.

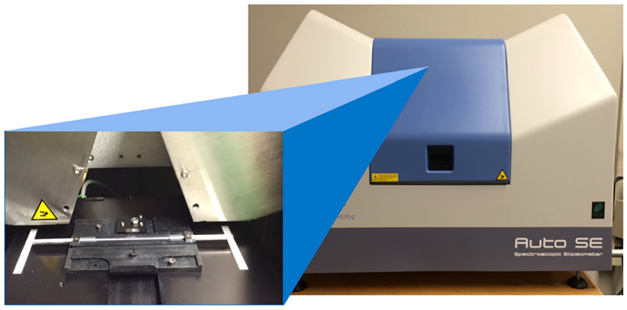

Fig. 5 Horiba Scientific Auto SE. The expanded view shows the tube mount on the positioning stage. The boxes on either side of the tube house the optical components to perform the ellipsometric measurement.

measured by the ellipsometer. Ellipsometry is named for this use of elliptically polarized light.

After preparation in the HLPS and analysis using the color standard, the completely cooled tube is placed into the ellipsometer shown in Fig. 5. All of the ellipsometric measurements are done at room temperature. There is a mount inside the ellipsometer to hold the tube in place. The mount is on a stage that can move in all three directions to position the sample.

Ellipsometry is an optical technique that uses changes in light polarization to determine the properties of a thin film. The film's thickness, composition, structure, and surface roughness can all be determined using ellipsometry; however, this study is concerned with the thickness because it can be correlated with thermal stability. When light crosses a boundary between two materials, the phase and intensity of the beam change. The light reflects and refracts according to Snell's Law, which is given in the following equation:

$$n_0 \sin\phi_i = n_1 \sin\phi_t \tag{5}$$

A portion of the incoming light is reflected from the surface at an angle equal to the angle of incidence. The remainder of the light transmits into the material at a refracted angle given by Snell's law (Fig. 6).

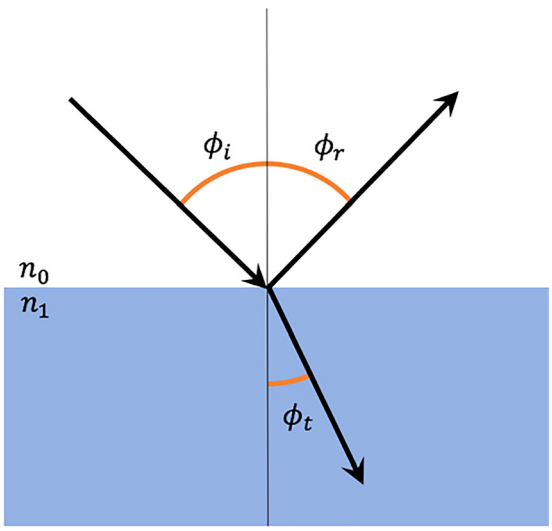

Fig. 6 Illustration of light reflection and refraction that occurs at an interface. A portion of the incoming light reflects at an angle equal to the angle of incidence, and the remainder is transmitted into the material at a refracted angle governed by Snell's law.

The light reflects and refracts at the contact plane between the two materials, and in a multilayer material, this occurs at each interface (see Fig. 7). This means that the overall reflected beam is made up of components from each interfacial interaction. The properties of this beam are tracked though each medium change, and in this way, the thickness can be determined using the Fresnel equations (Eq. (6)) where β is the phase change for a beam of light that passes twice through the material. In Eqs. (6), (9), and (10), the p superscript indicates that the equation pertains to the component of the light oscillating parallel to the plane of incidence, and the s superscript indicates that the equation pertains to the component oscillating perpendicular to the incidence plane

$$R^{p,s} = \frac{r_{12}^{p,s} + r_{23}^{p,s}\exp(-j2\beta)}{1 + r_{12}^{p,s} r_{23}^{p,s}\exp(-j2\beta)} \tag{6}$$

$$\beta = 2\pi\left(\frac{t}{\lambda}\right) N_2 \cos(\phi_2) \tag{7}$$

$$N_i = n_i - jk_i \tag{8}$$

$$r_{ij}^{p} = \frac{N_j \cos\phi_i - N_i \cos\phi_j}{N_j \cos\phi_i + N_i \cos\phi_j} \tag{9}$$

$$r_{ij}^{s} = \frac{N_i \cos\phi_i - N_j \cos\phi_j}{N_i \cos\phi_i + N_j \cos\phi_j} \tag{10}$$

Ellipsometry can be used to determine the thickness of thin films only. In this context, thin is defined to mean that at least a portion of the light that is incident on the sample reaches the substrate and returns back the ambient so that it is collected by the detector. If the light is entirely absorbed by the sample before reaching the ambient again, the information containing the thickness of the film is lost with the light. In Fig. 7, the second ray which returns to the white section satisfies this condition because the light gray section is the substrate.

The equations presented here are for a three component sample (the ambient, the film, and the substrate), but the same pattern can be extended for a different number of components to account for a film with multiple layers. N_i is the complex index of refraction, which is a convenient way of representing the index of refraction (n) and the coefficient of absorption (k). The $r_{ij}^{p,s}$ equations are the reflectance coefficients, which are ratios of the intensity of the incoming light to that of the outgoing for each individual layer,

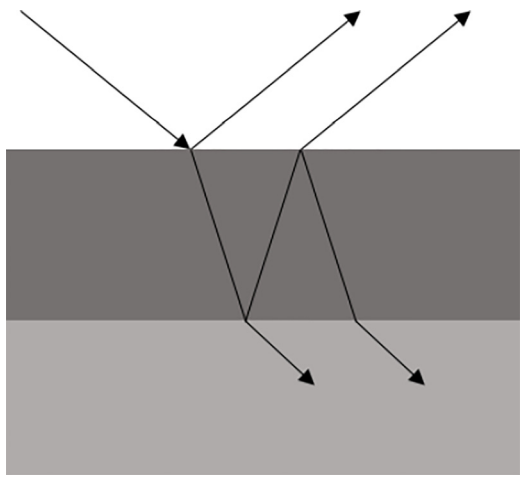

Fig. 7 Light behavior at an interface. The overall reflected beam is made up of components that come from each interfacial interaction.

and $R^{p,s}$ are the overall reflectance coefficients for the sample as a whole

$$\tan \Psi = \frac{|R^p|}{|R^s|} \tag{11}$$

$$\Delta = \text{phase of incoming light} - \text{phase of outgoing light} \tag{12}$$

$$\tan \Psi e^{i\Delta} = \frac{R^p}{R^s} \tag{13}$$

The ellipsometer measures Ψ, which is the ratio of the magnitude of the reflectance coefficients as shown in Eq. (11), as well as Δ which is the phase difference between the incoming and outgoing light beams. Ψ and Δ are measured over a range of wavelengths, and these points constitute the experimental data. Then, optical models are used to obtain theoretical n and k values over the same wavelength range. Equations (6)–(10) are used with the theoretical optical constants to produce theoretical reflectance coefficients with an assumed thickness, which are further used in Eqs. (11) and (13) to obtain theoretical Ψ and Δ values. The theoretical Ψ and Δ are compared to the experimental results, and the parameter χ^2 is used to quantify the adequacy of the fit (the lower the χ^2 the closer the fit). The guessed thickness value is incremented, and the process is iterated until a satisfactory χ^2 is found. The thickness at which the lowest χ^2 occurs is accepted as the thickness at that tube location. This process is repeated for 29 points, spaced 2 mm apart down the length of the tube to yield the thickness profile.

Reference materials were used to model the aluminum tubes. Reference materials are tables of the optical constants n and k for a particular material versus wavelength. The benefit of this approach is that it reduces the number of fitting parameters because each wavelength has a set n and k; however, it also makes the model less flexible for this same reason. Reference materials were chosen for this application because aluminum and aluminum oxide are widely studied materials with well-known optical properties. The reference files used here were created by Horiba Jovin Yvonne, a company based in France that created and supports the DELTAPSI2 software used in this study. The aluminum tube with deposit model is composed of a substrate layer of aluminum beneath a layer of aluminum oxide. A roughness layer was incorporated in the model on top of the aluminum oxide layer. This layer is composed of 50% aluminum oxide and 50% empty space, or void, giving it the optical properties of a mixture of the two. This is a standard method for representing a roughness layer.

A new amorphous dispersion formula was used to model the deposits on the stainless steel tubes. This model has a base substrate layer of stainless steel with a hydrocarbon film layer on top. A dispersion formula is used when it is desirable to be able to fit the optical constants as well as the film thickness. The new amorphous dispersion is described by Eqs. (14)–(18) [22]

$$k(\omega) = \sum_{j=1}^{N} \frac{f_j(\omega - \omega_g)^2}{(\omega - \omega_j)^2 + \Gamma_j^2} \quad \text{for } \omega > \omega_g \tag{14}$$

$$k(\omega) = 0 \quad \text{for } \omega \le \omega_g \tag{15}$$

$$n(\omega) = n_\infty + \sum_{j=1}^{N} \frac{B_j(\omega - \omega_j) + C_j}{(\omega - \omega_j)^2 + \Gamma_j^2} \tag{16}$$

$$B_j = \frac{f_j}{\Gamma_j}\left[\Gamma_j^2 - (\omega_j - \omega_g)^2\right] \tag{17}$$

$$C_j = 2f_j\Gamma_j(\omega_j - \omega_g) \tag{18}$$

In these equations, ω is the photon energy (which can be converted to wavelength) of the incident light in electron volts (eV). In Eqs. (14) and (15), k is the coefficient of extinction of the film. This parameter is related to the absorption coefficient and determines how quickly light is absorbed by a material. ω_g is the photon energy at which the coefficient of extinction is first nonzero, and it is a significant parameter in describing the shape of the k curve. From Eq. (16), n is the index of refraction, which is the ratio of the speed of light in a vacuum to the speed of light in the film. Other major parameters are ω_j, n_∞, f_j, and Γ_j. The counter variable j ranges from 1 to N, where N is the number of peaks in the k curve. These parameters are shown graphically for curves with a single peak in Fig. 8.

ω_j is the photon energy where the jth peak occurs in the k curve, Γ_j is proportional to the full width at half maximum, and f_j is proportional to the height of the peak. The parameter n_∞ is the value of the index of refraction as the energy of the incident light approaches infinity. These parameters are used to describe the shape of the optical constant curves and it is important to define them because the goal of this model is to match the experimentally obtained data from the ellipsometer. These are the parameters that can be tuned to affect the fit.

Figure 9 shows the thickness profile of a representative tube along with a picture of that same tube to show how the thickness profile and discoloration on the surface correlate. The deposit is located on the right side of the tube, as shown by the thicker section of the deposit profile. Just to the left of the halfway point the deposit is no longer visible; however, a thin layer is still present as can be seen in the thickness profile. This highlights a benefit of the ellipsometric method as opposed to the color standard.

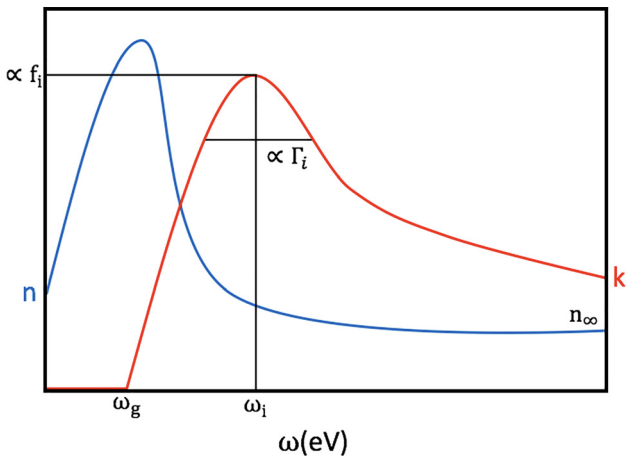

Fig. 8 Example optical constant spectrum with a single peak. The important parameters for the new amorphous dispersion are indicated.

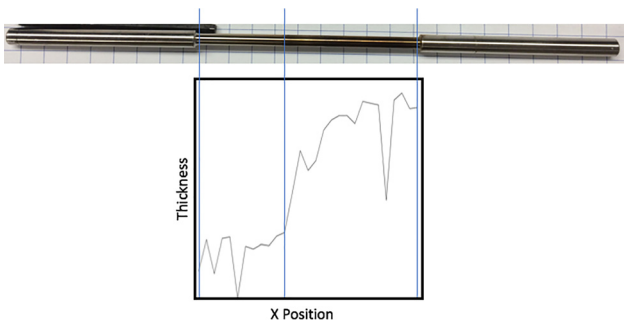

Fig. 9 Tube discoloration and thickness profile. Thicker deposition leads to more discoloration (however there is deposit present on the section that is not discolored).

Table 1 Aluminum results summary

Tube number	Test temperature (°C)	Fuel	Average χ^2	Thickness pass/fail	Max thickness (nm)	Deposit volume (mm^3)	JFTOT color pass/fail
1304	300	N118 SASOL IPK (100 vol %)	4.07	P	35.77	0.0112	1 (P)
1305	320	N118 SASOL IPK (100 vol %)	7.46	P	20.16	0.0088	1 (P)
1306	360	N118 SASOL IPK (100 vol %)	23.88	P	41.29	0.0143	1 (P)
1310	380	N136 SASOL IPK-1-M-Napthalene (99-1 vol %)	41.37	P	49.60	0.0219	1 (P)
1321	300	N138 SASOL IPK-1-M-Napthalene (95-5 vol %)	22.24	P	21.56	0.0087	1 (P)
1322	300	N138 SASOL IPK-1-M-Napthalene (95-5 vol %)	28.71	P	46.08	0.0143	<2 (P)
1327	380	N139 SASOL IPK-1,2,3,4-T-Napthalene (97-3 vol %)	39.18	P	46.93	0.0177	1 (P)
1330	345	N140 SASOL IPK-1,2,3,4-T-Napthalene (97-3 vol %)	33.13	P	49.53	0.0213	1 (P)
1335	380	N118 SASOL IPK (100 vol %)	30.29	P	28.82	0.0115	1 (P)
1337	380	N136 SASOL IPK-1-M-Napthalene (99-1 vol %)	31.50	P	46.25	0.0128	1 (P)
1344	340	N137 SASOL IPK-1-M-Napthalene (97-3 vol %)	11.24	P	12.90	0.0057	1 (P)

Aspects of the film that are not visible to the eye can be analyzed using ellipsometry while the color standard method relies only on the capabilities of the human eye. Absolute maximum thicknesses as well as total deposit volumes are presented in this study. The deposit volume is calculated assuming that the thickness profile is constant around the circumference of the tube.

Results and Discussion

Aluminum tubes exposed to Sasol IPK with varying levels of naphthalene were analyzed over a fuel temperature range of 300–380 °C. The results are summarized in Table 1. All the tubes achieved a passing rating on the JFTOT color test of 1 or <2. Also, they achieved passing ratings using the ellipsometry thickness standard. Maximum deposit thicknesses as well as well as total deposit volumes are shown in Table 1.

Effect of Increasing Temperature: Aluminum. As the temperature of the fuel increases, the deposit thickness is expected to also increase. This is because at higher temperatures, the reactions that are breaking down the fuel would be occurring faster, and more of them would be occurring, leading to increased deposit levels. Tubes 1304, 1305, 1306, and 1335 span a fuel temperature range from 300 to 380 °C, all with 0% naphthalene. The maximum thicknesses and the deposit volumes for these tubes do not follow the expected monotonically increasing trend. This could be due to irregularities in the metal tube surface, and this fact highlights the importance of measuring the tube surface profile prior to exposing the tube to the fuel. Tubes 1344, 1330, and 1327 over a test temperature range of 340–380 °C with 3% naphthalene also do not show this trend. Between the lowest and highest temperature, the deposit thickness and volume do indicate increases in this case. Interestingly both sets show deposit peaks (in maximum thickness and deposit volume) at similar temperatures (345 and 360 °C, respectively). Further investigation is necessary to understand the mechanism breaking down the fuel in this temperature range contributing to the deposit peak.

Repeatability: Aluminum. Tubes 1321 and 1322 were tested at the same fuel temperature, 300 °C, and with the same naphthalene concentration, 5%; however, the maximum thicknesses and total deposit volumes for these samples are quite different with a more than 100% difference in maximum thickness and more than 50% difference in volume. It is possible that these differences may be attributable to surface differences in the substrates and not the deposits themselves, but it is not possible to know this without measuring the surface profile of the tube before exposing it to the fuel. Tubes 1337 and 1310 were also tested with identical conditions (380 °C and 1% naphthalene). The maximum thicknesses show much closer agreement in this case (46.25 and 49.60 nm, respectively). It is, however, interesting to note the differences in total deposit volume between these two samples. This suggests that while the two had similar peak thicknesses, one profile was thicker on average to produce the greater volume. Reporting only the maximum thickness as is required by ASTM D3241 may not provide adequate representation of a fuel's thermal stability.

Effect of Increasing Naphthalene: Aluminum. Figures 10 and 11 show two representative thickness profiles for these measurements. Tubes 1304, 1321, and 1322 were all tested at a fuel temperature of 300 °C with varying naphthalene concentration from 0% to 5%. Tubes 1321 and 1322 are repeated verifications as noted previously; however, it is difficult to make comments about the effect of the naphthalene because depending on which 5% tube is chosen, opposite trends are seen. In the case of tubes 1335 and 1337 at 380 °C and 0% and 1% naphthalene, respectively, as the concentration of naphthalene increases, the maximum deposit thickness increases dramatically. However, if the total deposit volume is examined, it is found that the total deposit increases minimally with the increased naphthalene. This again highlights the fact that maximum thickness does not provide a complete picture of the fuel's behavior, and that both deposit volume and maximum thickness should be considered. It must be emphasized here that all of the previously mentioned comparisons would have been impossible to make with only data obtained from the color standard (as in the traditional JFTOT).

Stainless steel tube substrates were exposed to Sasol IPK over a temperature range of 385–400 °C with 0–5% naphthalene by volume. The results are summarized in Table 2. All of these tubes failed the color test for thermal stability. Additionally, all of these

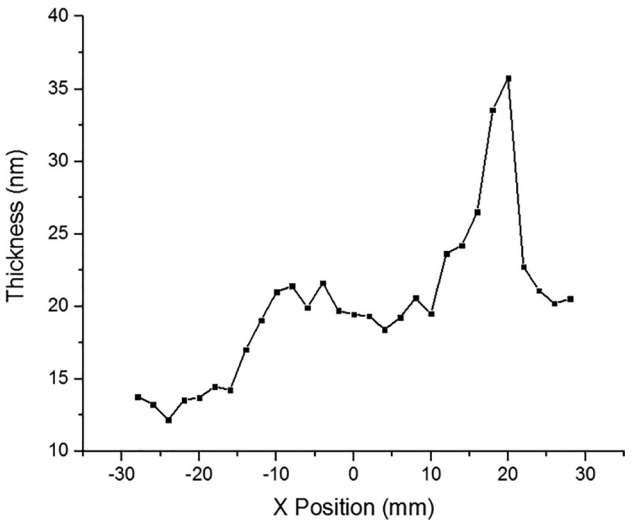

Fig. 10 Tube 1304 thickness profile. This tube was exposed to Sasol IPK with 0% naphthalene at 300 °C, yielding a maximum deposit thickness of 35.77 nm and a deposit volume of 0.0112 mm^3.

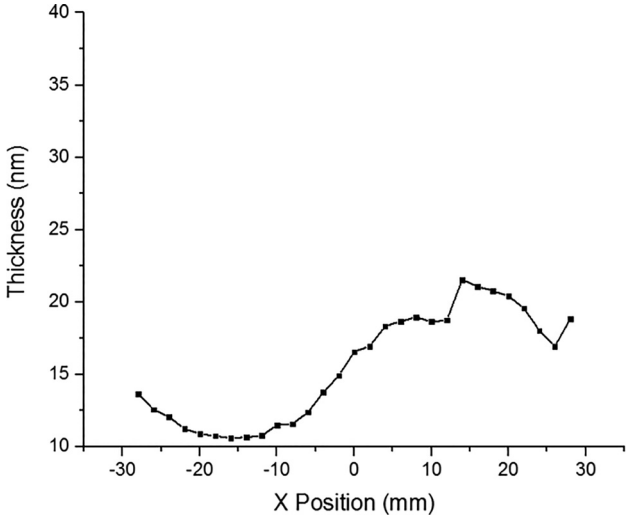

Fig. 11 Tube 1321 thickness profile. This tube was exposed to Sasol IPK with 5% naphthalene, yielding a maximum deposit thickness of 21.56 nm and a deposit volume of 0.0087 mm^3.

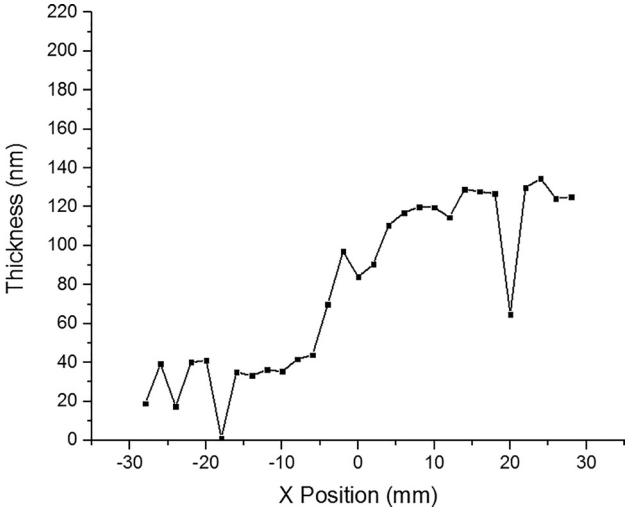

Fig. 12 Tube 1311 thickness profile. This tube was exposed to Sasol IPK with 1% naphthalene at 385 °C, yielding a maximum deposit thickness of 134.51 nm and a deposit volume of 0.0438 mm^3.

tubes resulted in maximum thicknesses that would rate them as thermally unstable (>85 nm). It is not surprising that the stainless steel tubes all failed the color test because the color standard is only applicable to aluminum tubes. It is, however, worth analyzing these tubes further, because as was seen with the aluminum tubes earlier, subtle differences are present that are not immediately noticeable.

Effect of Increasing Temperature: Stainless Steel. The deposit amount is also expected to increase with temperature for the stainless steel cases (as was expected for the aluminum cases mentioned previously). Tubes 1309 and 1308 agree with this hypothesis in maximum deposit thickness. Tubes 1311 and 1329 were tested at fuel conditions of 385 °C and 1% naphthalene. Tube 1328 was also exposed to 1% naphthalene, but at 400 °C. Between tubes 1311 and 1328; the deposit thickness increases; however, between tubes 1329 and 1328, it decreases with the increase in temperature. In this case, it is instructive to consider the deposit volume. The volumes for the two tubes at 385 °C are similar (0.0438 mm^3 and 0.0489 mm^3, respectively), as would be expected for identical test conditions. The volume for the tube at 400 °C increases to 0.1396 mm^3. This also agrees with the initial hypothesis. This highlights the need to examine not only the peak deposit thickness but the total deposit volume as well.

Considering tubes 1309, 1308, 1311, and 1328, the increase in maximum deposit thickness is greater for the 0% naphthalene tubes; however, the range here is also larger. If the increase in thickness is assumed to be linear, then for an equal increase in temperature the deposit thickness with 1% naphthalene increases more. It should be noted that this linearization is only an approximation, but in the absence of other data on this fuel it is an acceptable assumption to make. Figures 12 and 13 show representative thickness profiles for the stainless steel cases.

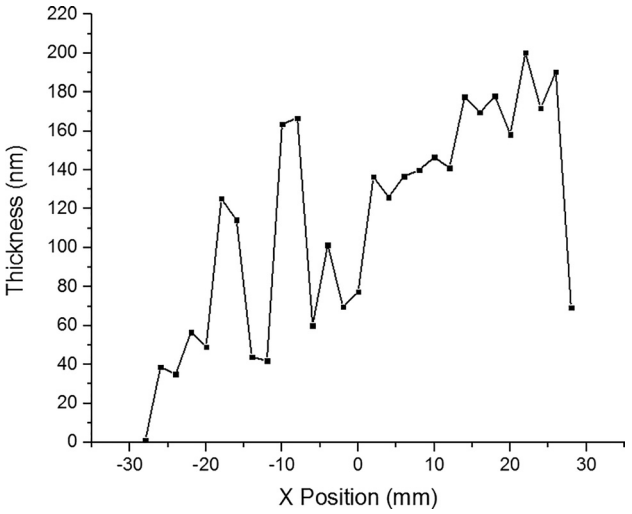

Fig. 13 Tube 1328 thickness profile. This tube was exposed to Sasol IPK with 1% naphthalene at 400 °C, yielding a maximum deposit thickness of 200.24 nm and a deposit volume of 0.0649 mm^3.

Repeatability: Stainless Steel. Tubes 1311 and 1329 were tested at a fuel temperature of 385 °C and 1% naphthalene. These

Table 2 Stainless steel results summary

Tube number	Test temperature (°C)	Fuel	Average χ^2	Thickness pass/fail	Max thickness (nm)	Deposit volume (mm^3)	JFTOT color pass/fail
1308	390	N118 SASOL IPK (100 vol %)	0.30	F	206.32	0.041	4 (F)
1309	385	N118 SASOL IPK (100 vol %)	0.28	F	137.07	0.0411	3 (F)
1311	385	N136 SASOL IPK-1-M-Napthalene (99-1 vol %)	0.18	F	134.51	0.0438	4 (F)
1328	400	N139 SASOL IPK-1,2,3,4-T-Napthalene (99-1 vol %)	0.39	F	200.24	0.0649	4 (F)
1329	385	N139 SASOL IPK-1,2,3,4-T-Napthalene (99-1 vol %)	0.22	F	212.39	0.0489	4 (F)
1332	385	N140 SASOL IPK-1,2,3,4-T-Napthalene (97-3 vol %)	0.25	F	189.96	0.0522	4 (F)
1333	385	N141 SASOL IPK-1,2,3,4-T-Napthalene (95-5 vol %)	0.27	F	452.92	0.0678	4 (F)
1339	385	N136 SASOL IPK-1-M-Napthalene (99-1 vol %)	0.14	F	132.58	0.0241	3 (F)

tubes yielded maximum thicknesses of 134.51 and 212.39, respectively. Some of this difference could be caused by surface differences in the steel substrate. Here, it is again useful to look at the total deposit volumes which are 0.0438 and 0.0489 mm^3, suggesting an acceptable level of repeatability in the deposit volume measurement. This also indicates the sensitivity of the peak deposit thickness to some unknown factor that the deposit volume is not sensitive to. This may make the deposit volume a more useful measure of thermal stability.

Effect of Increasing Naphthalene: Stainless Steel. Tubes 1309, 1311, 1329, 1332, and 1333 were all tested at 385 °C. The test fuels for these tubes range from 0% to 5% naphthalene. As the naphthalene concentration increases, the maximum thickness does not show a clear trend. The deposit volume on the other hand increases as the concentration of naphthalene increases. This suggests that the naphthalene could be having a negative impact on the thermal stability of the Sasol IPK as was seen for the aluminum tubes.

Conclusions

In conclusion, it was demonstrated using ellipsometry that increasing temperature slightly increases the amount of deposit formed from Sasol IPK with varying levels of naphthalene on aluminum and stainless steel tubes. Although all the aluminum tubes received passing ratings and all the stainless steel tubes received failing ratings from both the JFTOT color standard test and the ellipsometry thickness criteria, far more information is gathered about the tubes when they are tested using ellipsometry. None of the results shown here would have been measureable without the ellipsometric method.

Changes in deposition that are not visible to the eye are detectable with an ellipsometer, which leads to more in-depth understanding of the details of how an additive such as naphthalene affects a fuel. Also, this provides a screening method for selecting the most promising alternative jet fuel compounds. This work showed that peak deposit thickness may not be the best measure of thermal stability of a fuel, and that deposit volume should also be considered.

Effort is currently being undertaken to characterize the thermal stability of various alternative jet fuels and additives using ellipsometry. Future work in this area will focus on validating the thickness measurements using scanning electron microscopy and further refinement to the optical models used.

Acknowledgment

This material is based upon work supported by the National Aeronautics and Space Administration under Grant No. NNX15AU28H issued through the NASA Education Minority University Research Education Project (MUREP) through the NASA Harriett G. Jenkins Graduate Fellowship activity. The authors thank Michelle Sestak and Celine Eypert of Horiba Scientific for their assistance.

Nomenclature

ASTM = American Society for Testing and Materials
eV = electron volts
f_j = height of jth peak of the coefficient of extinction curve
HLPS = hot liquid process simulator
IPK = iso paraffinic kerosene
j = the imaginary number
JFTOT = jet fuel thermal oxidation test
k = coefficient of extinction
n = index of refraction
N = complex index of refraction
n_∞ = value of the index of refraction as wavelength approaches infinity
R^p = total reflectance coefficient in the direction parallel to the light propagation direction
R^s = total reflectance coefficient in the direction perpendicular to the light propagation direction
$r_{ij}^{p,s}$ = reflectance coefficient between the ith and jth surface in the parallel or perpendicular direction, respectively
t = thickness
β = phase change through one layer of film
Γ_j = the full width at half maximum of the jth peak of the coefficient of extinction curve
Δ = phase change across the sample
λ = wavelength
ϕ = angle between the light beam and the sample normal
χ^2 = goodness of fit parameter
Ψ = ratio of the total reflectance coefficients
ω = photon energy
ω_g = photon energy at which the coefficient of extinction is first nonzero
ω_j = photon energy of peak of the coefficient of extinction curve

References

[1] Vasu, S. S., Davidson, D. F., and Hanson, R. K., 2008, "Jet Fuel Ignition Delay Times: Shock Tube Experiments Over Wide Conditions and Surrogate Model Predictions," Combust. Flame, **152**(1–2), pp. 125–143.
[2] Colket, M., Edwards, T., Williams, S., Cernansky, N. P., Miller, D. L., Egolfopoulos, F., Lindstedt, P., Seshadri, K., Dryer, F. L., Law, C. K., Friend, D., Lenhert, D. B., Pitsch, H., Sarofim, A., Smooke, M., and Tsang, W., 2007, "Development of an Experimental Database and Kinetic Models for Surrogate Jet Fuels," AIAA Paper No. 2007-770.
[3] Colket, M. B., Heyne, J., Rumizen, M., Edwards, J. T., Gupta, M., Roquemore, W. M., Moder, J. P., Tishkoff, J. M., and Li, C., 2016, "An Overview of the National Jet Fuels Combustion Program," AIAA Paper No. 2016-0177.
[4] Colket, M., Heyne, J., Rumizen, M., Gupta, M., Edwards, T., Roquemore, W. M., Andac, G., Boehm, R., Lovett, J., Williams, R., Condevaux, J., Turner, D., Rizk, N., Tishkoff, J., Li, C., Moder, J., Friend, D., and Sankaran, V., 2017, "Overview of the National Jet Fuels Combustion Program," AIAA J., **55**(4), pp. 1087–1104.
[5] Temme, J., Coburn, V., and Kweon, C.-B., 2017, "High-Speed Chemiluminescence Measurements of Alternative Jet Fuels at Engine Relevant Ambient Conditions," AIAA Paper No. 2017-0151.
[6] Bora, B. J., and Saha, U. K., 2016, "Estimating the Theoretical Performance Limits of a Biogas Powered Dual Fuel Diesel Engine Using Emulsified Rice Bran Biodiesel as Pilot Fuel," ASME J. Energy Resour. Technol., **138**(2), p. 021801.
[7] West, R., and Kreith, F., 2006, "A Vision for a Secure Transportation System Without Hydrogen or Oil," ASME J. Energy Resour. Technol., **128**(3), pp. 236–243.
[8] Barari, G., Koroglu, B., Masunov, A., and Vasu, S. S., 2016, "Products and Pathways of Aldehydes Oxidation in the Negative Temperature Coefficient Region," ASME J. Energy Resour. Technol., **139**(1), p. 012203.
[9] Barari, G., Pryor, O., Koroglu, B., Lopez, J., Nash, L., Sarathy, S. M., and Vasu, S. S., 2017, "High Temperature Shock Tube Experiments and Kinetic Modeling Study of Diisopropyl Ketone Ignition and Pyrolysis," Combust. Flame, **177**, pp. 207–218.
[10] Almansour, B., Alawadhi, S., and Vasu, S., 2017, "Laminar Burning Velocity Measurements in DIPK—An Advanced Biofuel," SAE Int. J. Fuels Lubr., **10**(2), p. 2017-01-0863.
[11] McCormick, R. L., Fioroni, G., Fouts, L., Christensen, E., Yanowitz, J., Polikarpov, E., Albrecht, K., Gaspar, D. J., Gladden, J., and George, A., 2017, "Selection Criteria and Screening of Potential Biomass-Derived Streams as Fuel Blendstocks for Advanced Spark-Ignition Engines," SAE Int. J. Fuels Lubr., **10**(2), p. 2017-01-0868.
[12] Willette, P. J., Shaffer, B., and Samuelsen, G. S., 2015, "Systematic Selection and Siting of Vehicle Fueling Infrastructure to Synergistically Meet Future Demands for Alternative Fuels," ASME J. Energy Resour. Technol., **137**(6), p. 062204.
[13] Quintero, S. A., Schmitt, J., Blair, R., Nash, D., and Kapat, J. S., 2013, "Comparison of Thermal Stability Characteristics of Fischer-Tropsch and Hydroprocessed Alternative Jet Fuels in a Fixed Bed Reactor," ASME Paper No. GT2013-95041.
[14] ASTM, 2015, "Standard Test Method for Thermal Oxidation Stability of Aviation Turbine Fuels," American Society for Testing and Materials, West Conshohocken, PA, Standard No. ASTM D3241-08.
[15] Baker, C., David, P., Taylor, S., and Woodward, A., 1995, "Thickness Measurement of JFTOT Tube Deposits by Ellipsometry," Fifth International Conference on Stability and Handling of Liquid Fuels, Rotterdam, The Netherlands, Oct. 3–7, pp. 433–447.
[16] Browne, S. T., Wong, H., Hinderer, C. B., and Klettlinger, J., 2012, "Enhancement of Aviation Fuel Thermal Stability Characterization Through Application of Ellipsometry," NASA Lewis Research Center, Cleveland, OH, Technical Report No. 2012-217404.

[17] Hui, X., Kumar, K., Sung, C.-J., Edwards, T., and Gardner, D., 2012, "Experimental Studies on the Combustion Characteristics of Alternative Jet Fuels," Fuel, **98**, pp. 176–182.
[18] Moses, C. A., 2008, "Comparative Evaluation of Semi-Synthetic Jet Fuels," Universal Technology Corporation, Dayton, OH, Contract No. F33415-02-D-2299.
[19] Dryer, F. L., Ju, Y., Brezinsky, K., Santoro, R. J., Litzinger, T. A., and Sung, C.-J., 2012, "Generation of Comprehensive Surrogate Kinetic Models and Validation Databases for Simulating Large Molecular Weight Hydrocarbon Fuels," Defense Technical Information Center, Fort Belvoir, VA, DTIC Document No. ADA578384.
[20] Yu, G., Askari, O., Hadi, F., Wang, Z., Metghalchi, H., Kannaiyan, K., and Sadr, R., 2017, "Theoretical Prediction of Laminar Burning Speed and Ignition Delay Time of Gas-to-Liquid Fuel," ASME J. Energy Resour. Technol., **139**(2), p. 022202.
[21] Lindsey, J., and Klettlinger, S., 2013, "Thermal Stability Results of a Fischer-Tropsch Fuel With Various Blends of Aromatic Solution," NASA Lewis Research Center, Cleveland, OH, Technical Report No. 2012-216019.
[22] Zhang, H. R., Eddings, E. G., and Sarofim, A. F., 2007, "Alias: Utah Surrogate Mechanism: Zhang's MECOFU Version 403 Beta," Proc. Combust. Inst., **31**(1), pp. 401–409.